PAPER

Absorption efficiency of the second harmonic ECRH waves and comparative plasma transport simulation in the TJ-II stellarator and T-10 tokamak

To cite this article: Yu N Dnestrovskij *et al* 2023 *Plasma Phys. Control. Fusion* **65** 015011

IOP Publishing Plasma Physics and Controlled Fusion
Plasma Phys. Control. Fusion **65** (2023) 015011 (13pp) https://doi.org/10.1088/1361-6587/aca35a

Absorption efficiency of the second harmonic ECRH waves and comparative plasma transport simulation in the TJ-II stellarator and T-10 tokamak

Yu N Dnestrovskij[1,*], A V Melnikov[1,2,3], D Lopez-Bruna[4], A Yu Dnestrovskij[1], S V Cherkasov[1], A V Danilov[1], L G Eliseev[1], P O Khabanov[1], S E Lysenko[1] and D Yu Sychugov[5]

[1] National Research Center 'Kurchatov Institute', Moscow, Russia
[2] National Research Nuclear University 'MEPhI', Moscow, Russia
[3] Moscow Institute of Physics and Technology, Dolgoprudny, Russia
[4] Laboratorio Nacional de Fusion, CIEMAT, Madrid, Spain
[5] Moscow State University, Moscow, Russia

E-mail: Dnestrovskiy_YN@nrcki.ru

Received 22 June 2022, revised 19 October 2022
Accepted for publication 16 November 2022
Published 7 December 2022

Abstract

The concept of equivalent tokamak and stellarator discharges with the same electron and ion temperatures and with full absorption of the injected ECRH power was introduced in Dnestrovskij *et al* (2021 *Plasma Phys. Control. Fusion* **63** 055012). In the present paper, the concept of the discharges equivalence is extended to the case of partial ECRH power absorption. The conditions of discharges equivalence for this case are formulated. It is shown that in equivalent discharges not only the electron temperatures, but also the absorbed powers are the same. Examples of equivalent experimental discharges of the TJ-II stellarator and simulated discharges of the T-10 tokamak with partial ECRH power absorption are studied. The absorbed ECRH power and energy confinement time are found for TJ-II low-density shots heated with ECRH only.

Keywords: tokamak, stellarator, electron cyclotron resonance heating (ECRH), transport, numerical simulation, equivalent discharges, inverse problems

(Some figures may appear in colour only in the online journal)

1. Introduction

Comparing energy transport between tokamak and stellarator plasmas is an important topic in fusion studies. The first attempt to construct a common scaling for the energy confinement time τ_E in these devices was performed in [1]. The main difficulty in constructing such a scaling consists in the way the poloidal magnetic field B_p is created in the plasma. In a tokamak, the field B_p is excited by a large toroidal current I. In a stellarator, most of this field is induced by currents in external conductors.

In order to standardize the data, they replaced in the tokamak scaling laws the plasma current by the dimensionless edge safety factor $q(a) \approx a^2 B/(0.2IR)$, where B is the toroidal magnetic field at the plasma axis and a and R are the minor and major radii of the torus; q describes the helicity of the magnetic field lines on the flux surfaces. Historically, q was

* Author to whom any correspondence should be addressed.

used in tokamaks, while traditionally in stellarators the inverse value—the rotational transform $\iota = 1/q$ was conventionally used. Therefore, it seems natural to unify scaling laws for tokamaks and stellarators using the same parameter describing the helicity of the plasma, for which they choose $q(a)$.

However, in [1] it becomes clear that at the same helicity, the heat flows in the tokamak and the stellarator are not the same. Indeed, using the ratio $q(a) = 1/\iota(a)$ in the scaling law, one can see that the stellarator transport is much worse than the tokamak one. Analysis of the energy transport in a tokamak using a critical gradient transport model [2] showed that the right hand side of this ratio should be increased by some factor [3]. In [4] we determine this factor and use the following relation:

$$q(a) = 2\pi/\iota(a). \tag{1}$$

Note that edge safety factor $q(a)$ has a strict low limit in tokamaks because of the Kruscal-Shafranov condition for the plasma macroscopic stability, but $\iota(a)$ has no such limit and can be very different for different stellarators. In particular, for the W-7X stellarator, $\iota(a)$ varies in the range of $0.8 < \iota(a) < 1.2$ [5]. For the TJ-II stellarator we take $\iota(a) = 1.56$.

Plasma heating using ECR waves at the second harmonic X-mode (X2 ECRH) is discussed in [4], where criteria for full or partial absorption were derived, the concept of equivalent pairs of tokamak and stellarator discharges was introduced, and the necessary and sufficient conditions for equivalence were formulated. As an example of equivalent pairs, we have used, on one hand, experimental discharges from the W7-X stellarator, and, on the other hand, the modelling results for the T-15MD tokamak using the Standard transport model of canonical profiles (STMCP). Remarkably, the electron and ion temperatures in the corresponding discharge pairs were pairwise identical.

In this paper, we present the results of similar studies for several pairs of equivalent discharges from the TJ-II stellarator and the T-10 tokamak. Both the TJ-II and T-10 discharges undergo partial absorption of ECRH power, requiring modifications in the equivalence conditions and the data processing algorithms used in [4].

In T-10, we found that with X2 ECR heating, all of the heating energy is absorbed for some plasma scenarios, but only part of it for others [6]. This raises the question of how to construct a transport model that would both determine the mode of absorption and allow the modelling of the plasma at both full and partial absorption.

Until the early 1990s, T-10 has been using ECRH in O-Mode at the first harmonic, the so-called O1-mode, characterized by full power absorption. Based on these experiments, the STMCP was developed. The current state of development is described in [4], and the main set of formulas is given in appendix A.

When using X2 ECRH, the modelling of T-10 discharges with the STMCP sometimes encountered difficulties, more in particular, the modelled electron temperatures were overestimated compared to the experimental temperatures, especially for low-density plasmas. This led to the suggestion that the ECRH power was only partially absorbed, and the new task arose to determine the ECRH power absorbed by a plasma with a given $T_e(r)$ profile. To solve it, in principle, one should solve the inverse coefficient problem for the parabolic heat transport equation.

Therefore, the procedure of transport modelling has the following alternative. If the ECRH power is fully absorbed, one should solve the direct problem using the STMCP and determine $T_e(r)$. If the power is only partially absorbed, then the inverse problem for the STMCP should be solved, in order to determine the absorbed power by $T_e(r)$ as an input data.

For many decades, transport models for the stellarator were based on neoclassical concepts of energy and particle transport, although it was also realized that the near-edge region was possibly anomalous [7]. Recent W7-X experiments have shown that plasma energy transport is not fully described by neoclassical models, but by turbulent fluxes or, generally speaking, non-neoclassical effects are dominant [8].

In the present paper, we start with the concept of equivalent discharges between stellarators and tokamaks as described in [4] and use the relations applicable to equivalent discharges. We consider discharges with full and partial absorption of the ECRH power and extend the concepts developed in [4] to partial absorption of ECRH power.

It is well known that the temperature profiles in stellarator have no self-consistency property [9]. This is the reason, why the canonical profile transport model is absent for stellarator. However, it is also known, that the electron pressure profiles in stellarator has such a property [10, 11]. The expression for the canonical pressure profiles was found in [11]. In addition, the on-axis ECRH makes the plasma density profile close to the flat one due to the pump-out effect. This means that the electron temperature profile in a stellarator at the ECRH is close to the canonical pressure profile, but does not coincide with it due to the ECRH as an auxiliary heating source. This is a basis for the opportunity of the comparison of electron temperature profiles in stellarator and tokamak.

The paper is organized as follows. In section 2, the discharge equivalence with full ECRH power absorption is considered, while the case of partial absorption is described in section 3. The inverse problem for determining the absorbed power profile and the regularization procedure are considered here. The TJ-II stellarator is described in section 4. In section 5, we choose several equivalent discharge pairs for TJ-II and T-10. In section 6, we present results of the inverse problem solution in the framework of the STMCP. In section 7, we present plasma parameters obtained from solution of inverse problem. In section 8, we propose an empirical formula for the ECRH efficiency. New data from TJ-II allow us to improve the formula presented in [4]. In section 9, we calculate the stored energy and confinement time in the equivalent tokamak and stellarator. In section 10, we discuss the L-mode plasma heated at the second harmonic of ECRH and the lack of plasma

volume requirements under equivalent conditions. Section 11 summarizes the main results.

2. Equivalent discharges for full absorption of ECRH power

We call stellarator and tokamak discharges as equivalent, if they meet the following requirements [4]:

(a) Equal line average density $\bar{n}$;
(b) The same type of ECR heating: on-axis;
(c) The same input heating power $Q_{\rm in}$ (the ECRH power $Q_{\rm EC}^{\rm st}$ in the stellarator discharge, the sum of the ECRH $Q_{\rm EC}^{\rm tok}$ and ohmic $Q_{\rm j}$ powers in the tokamak discharge, $Q_{\rm in} = Q_{\rm EC}^{\rm st} = Q_{\rm EC}^{\rm tok} + Q_{\rm j}$). We assume here that the input power $Q_{\rm in}$ is fully absorbed;
(d) Toroidal magnetic fields B with a difference smaller than 25%–30%.
(e) The value of edge safety factor $q(a)$ for tokamak discharge is about 2π times larger than the value of $1/\iota(a)$ for the stellarator discharge.

Note that these requirements are different from the original formulation [4] in point (c). We now include the ohmic power in the heating power of the tokamak. Transport modelling using STMCP for tokamak shows that for equivalent discharges the measured profiles of electron and ion temperatures in the stellarator are close to the corresponding modelled temperature profiles for the tokamak.

Note that the expression (1) differs from the definition of the safety factor and rotational transform at the plasma boundary: $q(a) = 1/\iota(a)$. This means that the temperature profiles (heat fluxes) in a stellarator discharge will approximate those in a corresponding tokamak discharge if the helicity of the magnetic field lines at the edge of the stellarator and tokamak differ by a factor of about 2π. Figure 1 shows TJ-II typical profiles of $\iota(\rho)$ for $\iota(a) = 1.6$ [12] and $2\pi/\iota(\rho)$ together with $q(\rho)$ profiles from T-10. For this case, condition (e) is satisfied at the plasma edge with $q(a) = 2\pi/\iota(a) \approx 4$. However, the radial profiles $2\pi/\iota(\rho)$ and $q(\rho)$ are very different in the plasma core. This means that the safety factor at the edge, and not the radial profile, is a key parameter responsible for the energy transport in the toroidal plasma.

Note that the concept of equivalence, defined above, does not include a comparison of the plasma volume and shape. Details of this topic will be discussed in section 10. Since the plasma volumes in equivalent discharges may be different, the global confinement characteristics such as stored energy or energy confinement time may also differ. In the absence of predictive transport models for stellarator plasmas, the identity of the temperature profiles in equivalent pairs of tokamak/stellarator discharges allows us to replace transport modelling (calculation of temperature) in the stellarator with modelling of the equivalent tokamak discharge using the STMCP verified against experiments in various machines [13, 14], as has been done for W7-X and T-15MD [4].

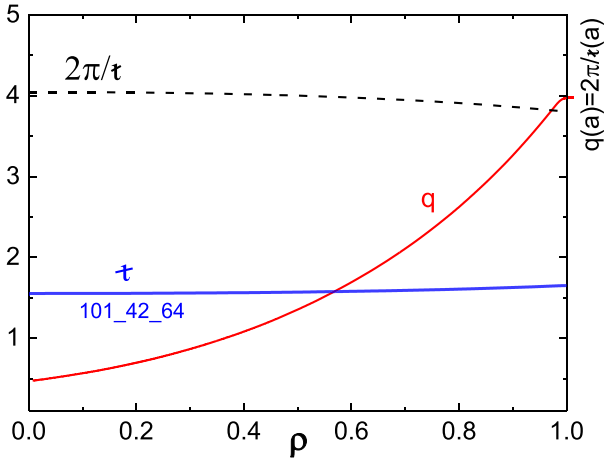

Figure 1. Comparison between the profile of the rotational transform ι together with the ratio $2\pi/\iota$ in the standard TJ-II magnetic configuration [12], and the typical safety factor q in T-10.

3. Equivalent discharges for partial ECRH power absorption

We call a pair of discharges from stellarator and tokamak with partial power absorption as equivalent, if they meet the equivalence requirements of section 2, except point (c), which is replaced by the following requirement:

(c) The same value of the absorbed power $Q_{\rm ab}^{\rm st} = Q_{\rm ab}^{\rm tok} = Q_{\rm ab}$, where $Q_{\rm ab}^{\rm st} = Q_{\rm abEC}^{\rm st}$ is the absorbed ECRH power in the stellarator discharge and $Q_{\rm ab}^{\rm tok} = Q_{\rm abEC}^{\rm tok} + Q_{\rm j}$ is the sum of the absorbed ECRH $Q_{\rm abEC}^{\rm tok}$ and ohmic power $Q_{\rm j}$ in the tokamak discharge. This implies that the electron and ion temperatures in the stellarator discharge are measured. The direct transport problem formulation is: to find the radial temperature profile with given coefficients of the energy transport equation (A11) including the energy source. There are many algorithms to solve this problem, for example, the successive factorization method.

The inverse transport problem formulation is: to find the power source in the transport equation (A11) with given electron temperature profile (for example, from the experiment). This inversed coefficient problem is an ill-posed one [15, 16].

By solving the inverse transport problem using the STMCP for equivalent discharges, we can determine the radial profile for the power absorbed by the electrons and find that the optimal electron temperature profile in the tokamak is close to the experimental electron temperature of the stellarator.

We use a relatively simple method for regularizing the profile of the power absorbed by the electrons. We are looking for an unknown power source within the class of trial functions characterized by a small number of free parameters. We then pose the direct problem with a selected given profile for the absorbed power and solve it, leading to a calculated electron temperature profile. Thus, we reformulate the inverse problem by a problem of minimizing the discrepancy between the calculated electron temperature and the given experimental electron temperature profile, equation (A12). The trial function minimizing the discrepancy is an optimal quasi-solution.

We assume multi-pass absorption for the second-harmonic EC waves at low plasma density [17]. Since the wall of the vacuum chamber is corrugated, the direction of propagation of the ECRH beam after reflection from the wall is unpredictable. Apparently, only a small fraction of the power of the ECRH beam is absorbed in the plasma after each reflection from the metal wall. This means that the ECRH beam passes multiple times through the plasma, and with each pass, part of its power will be absorbed at an unpredictable radius. We assume for the radial profile of the absorbed ECRH-power density P_{ab}, a Gaussian function with variable amplitude A, and half-width γ:

$$P_{ab} = A \exp\left(-\left(\frac{\rho}{2\gamma}\right)^2\right). \tag{2}$$

This description of P_{ab} is more suitable than the combination of flat and peaked functions used in [4].

The fitting parameters A and γ are found, when the calculated electron temperature profile $T_e(\rho)$ is as close as possible to the experimental electron temperature profile. For the sake of brevity, we refer to this best-fit temperature profile as "optimal". The smaller the deviation between the calculated and experimental temperature profiles, the better the approximation for P_{ab}. The solution of this problem is not necessarily unique; it depends on the class of allowable functions for P_{ab}. The chosen class of functions P_{ab}, as shown in equation (2), adequately reflects the ECRH power deposition [18], so that such a quasi-solution has sufficient accuracy for the subsequent transport analysis.

Note that for stellalator discharges with absorbed ECRH power density P_{ab}^{st}, the full absorbed power

$$Q_{ab}^{st} = Q_{ab\,EC}^{st} = \int_{Vst} P_{ab}^{st}\,dV \tag{3}$$

is only due to ECRH, while for tokamak discharges with absorbed ECRH power density P_{ab}^{tok}, the total absorbed power is the sum of the ECRH and ohmic heating power:

$$Q_{ab}^{tok} = Q_{ab\,EC}^{tok} + Q_j = \int_{Vtok} P_{ab}^{tok}dV + Q_j, \tag{4}$$

where V_{st} and V_{tok} are the plasma volumes for the stellarator and tokamak discharges. The values $Q_{ab}^{tok}$and P_{ab}^{tok} are determined by solving the inverse problem using the STMCP. However, due to requirements of the equivalency

$$Q_{ab}^{st} = Q_{ab}^{tok} = Q_{ab}. \tag{5}$$

It means that the absorbed ECRH power in stellarator discharge $Q_{ab\,EC}^{st}$ is larger than in the equivalent tokamak discharge $Q_{ab\,EC}^{tok}$, however converges to $Q_{ab\,EC}^{tok}$ as the contribution of Q_j decreases. We define the heating efficiency η as the ratio of the absorbed to the input power:

$$\eta^{st} = Q_{ab}/Q_{EC}, \tag{6a}$$

$$\eta^{tok} = Q_{ab}/(Q_{EC} + Q_j). \tag{6b}$$

4. Characteristics of the TJ-II stellarator

TJ-II is a stellarator with small magnetic shear and four periods for the magnetic field [12, 19]. The average values of the minor and major radii for the standard magnetic configurations are $a = 0.22$ m and $R = 1.5$ m. The toroidal magnetic field on the magnetic axis is $B = 1$ T. Plasma start-up and heating is done using ECRH at input power levels $Q_{EC}^{st} = 200$–500 kW, and neutral beam injection (NBI) with input power $Q_{NB} \leqslant 600$ kW for each of the two toroidally opposite injectors. These heating sources can be switched on separately. In the ECRH heating phase, the line average density is $\bar{n} = 0.3$–1×10^{19} m^{-3}, and typical central electron and ion temperatures are $T_e(0) = 0.8$–1.6 keV and $T_i(0) = 90$ eV. When using NBI, the plasma density increases significantly, and $T_e(0)$ decreases. At densities $\bar{n} = (2$–$5) \times 10^{19}$ m^{-3}, typical for NBI discharges, the electron temperature reaches $T_e(0) \sim 350$ eV and the ion temperature $T_i(0) \sim 120$ eV. In this paper, we exclude discharges with NBI heating.

5. Equivalent pairs for the TJ-II stellarator and T-10 tokamak shots

TJ-II electron temperature profiles have been determined and studied in e.g. [20–22]. Here, we selected six typical values for the line-averaged density and averaged the Thomson Scattering profiles for discharges in the database with the same ECRH power to reduce the statistical errors. The ion temperature profiles were not available and therefore they are not included. We arrange the selected shots in ascending order of average density and designate them by integers with the addition of the average density value. Table 1 summarizes the selected shots with symbolic numbers as well as with the line average density $\bar{n}^{exp}$, central electron temperature T_{ex0}, and the input ECRH power.

The actual discharge numbers used for the averaging in the symbolic shots are compiled in appendix B.

For the stellarator discharges, the electron density and temperature profiles are known and shown in section 7. The density profiles are sometimes slightly non-monotonic. The ECRH input power is equal to $Q_{EC}^{st} = 0.47$ MW, except the shot No. 5, where $Q_{EC}^{st} = 0.25$ MW.

Now we construct the tokamak shots that are equivalent for partial power absorption to the chosen stellarator shots. We will denote them in the same way as in table 1, but with the addition of the letter "t" at the end of their designation. As a basis, we take the T-10 parameters. The equivalence condition (e) requires the equality $q(a) = 2\pi/\iota(a)$. For all TJ-II shots, $\iota(a) = 1.56$, hence for tokamak shots $q(a) = 4$, see figure 1. For tokamak shots, we choose the same density as for the stellarator shots. To satisfy the conditions (b) and (c), we use the same ECRH heating scenario. The electron temperature profiles for TJ-II are experimentally determined.

To satisfy the requirement (d), we have to use tokamak discharges with a magnetic field B close to 1 T. However, such discharges are absent in the T-10 database, since usually, $B = 2.2$–2.4 T in T-10. Therefore, we design discharges for

Table 1. Selected shots from TJ-II and their designations.

Serial number	Line average density $\bar{n}^{exp}$, 10^{19} m^{-3}	Input ECRH power Q_{EC}^{st}, MW	Central electron temperature T_{ex0}, keV	Symbolic number
1	0.30	0.47	1.46	1030
2	0.47	0.47	1.58	2047
3	0.50	0.47	1.39	3050
4	0.70	0.47	1.31	4070
5	0.79	0.25	1.17	5079
6	0.90	0.47	1.31	6090

a virtual tokamak T-10V, which has the dimensions of T-10, but a much lower magnetic field $B = 1$ T. The temperature profiles for this virtual tokamak can be calculated using the STMCP, whose parameters were determined from the whole T-10 database ($1 < \bar{n}^{exp} < 4 \times 10^{19}$ m^{-3}). Note that STMCP has been verified on the MAST tokamak [14] with much lower magnetic field $B \sim 0.5$ T.

The plasma current for T-10V shots is determined in accordance to equivalence requirement (e):

$$q_{cyl} = \frac{5a^2B}{IR} = 4, \text{ thus } I = \frac{5a^2B}{4R} = 0.08 \text{ MA}. \quad (7)$$

In this way, the virtual tokamak T-10V ($R = 1.5$ m, $a = 0.3$ m, $B = 1$ T, $I = 0.08$ MA) fits all the requirements for equivalence with TJ-II.

6. Results of the inverse problem solution to determine the absorbed power profiles

Solving the inverse problem means that we have to determine the two parameters A and γ in equation (3) for P_{ab}, since all other parameters in the STMCP: h_e, C_e and μ_{0e} for electrons, h_i, C_i and μ_{0i} for ions are fixed, see table A1 in appendix A. Instead of A, we show the absorbed power Q_{ab} according to equation (4).

In table 2, the calculated parameters and values of Q_{ab} for the stellarator TJ-II based on the equivalent tokamak T-10V are shown together with the experimental T_{ex0} and optimal T_{e0} central electron temperatures. The root-mean-square (RMS) difference $d2T_e$ between the optimal electron temperature profile and the experimental profiles is below several percent.

Figure 2 shows the evolution of the central electron temperatures (both experimental and calculated) as a function of the average plasma density. The red circles represent the experimental temperature T_{ex0} for the TJ-II shots; the black squares represent the calculated temperature T_{e0} for the equivalent T-10V tokamak shots. Both T_{ex0} and T_{e0} have a weak tendency to decrease with increasing density.

In figure 2, we compare the dependencies of the experimental central electron temperature T_{ex0} for TJ-II discharges and the calculated optimal temperature T_e for the equivalent tokamak T-10V at $B = 1$ T (black squares) on the averaged plasma density. The straight line shows the threshold electron

Table 2. Calculated parameters for TJ-II shots based on the equivalent tokamak T-10V ($B = 1$ T) shots.

Symbolic number	γ	Input power Q_{EC}, MW	Q_{ab}^{st}, MW	η^{st}	T_{e0}, keV	T_{ex0}, keV	$d2T_e$, %
1030t	0.1	0.47	0.11	0.23	1.42	1.46	7.6
2047t	0.12	0.47	0.18	0.38	1.58	1.58	2.8
3050t	0.28	0.47	0.22	0.47	1.34	1.39	11
4070t	0.17	0.47	0.25	0.53	1.32	1.31	3.2
5079t	0.1	0.25	0.21	0.83	1.18	1.17	1.1
6090t	0.17	0.47	0.30	0.63	1.24	1.31	2.3

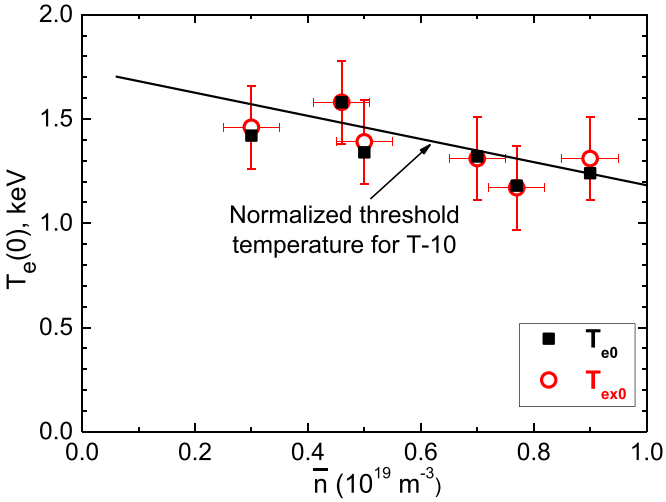

Figure 2. The dependence of the central experimental electron temperature T_{ex0} on the average plasma density for TJ-II (red circles) and the calculated optimal temperature T_{e0} for the equivalent tokamak T-10V at $B = 1$ T (black squares). The straight line is the threshold temperature, normalized to the magnetic field of T-10, $B = 2.4$ T.

temperature normalized to the magnetic field in T-10 (figure 3 in Ref. [4]), as a function of averaged density. The threshold temperature was introduced in [4] as a maximal electron temperature at certain density in the particular device over Q_{EC} variation. The slope of this line is determined by the balance between the increase of the electron temperature with increasing absorbed power and the decrease of temperature due to the increase in density. Remarkably, for both TJ-II and T-10, this evolution is the same.

7. Results obtained for the plasma parameter profiles

The following notations are used here:

T_e^{exp} is the experimental profile of the electron temperature in TJ-II;
n^{exp} is the experimental profile of the electron density in TJ-II;

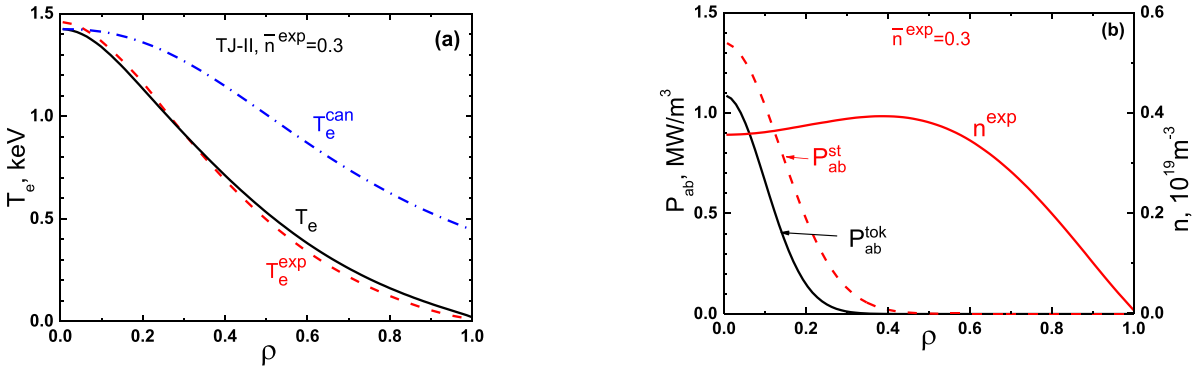

Figure 3. Results of the modelling for T-10V, based on the experimental values for TJ-II shot #1030 with $\bar{n}^{exp} = 0.3$. (*a*) Experimental electron temperature profile T_e^{exp}, (red dash line) for the shot #1030, calculated electron temperature profile T_e, (solid black line) for the shot #1030t and the canonical electron temperature profile T_e^{can}, (dash-dotted line). The RMS difference d2T$_e$ between T_e and T_e^{exp} is d2T_e = 7.6%; (b) Profiles of the experimental plasma density n^{exp} and the absorbed ECRH power densities P_{ab}^{st} ($\gamma = 0.11$) for TJ-II shot #1030 and P_{ab}^{tok} ($\gamma = 0.1$) for T-10V shot #1030t, the ohmic power $Q_j = 0.05$ MW, absorbed power $Q_{ab} = 0.11$ MW and the heating efficiency $\eta^{st} = 0.23$.

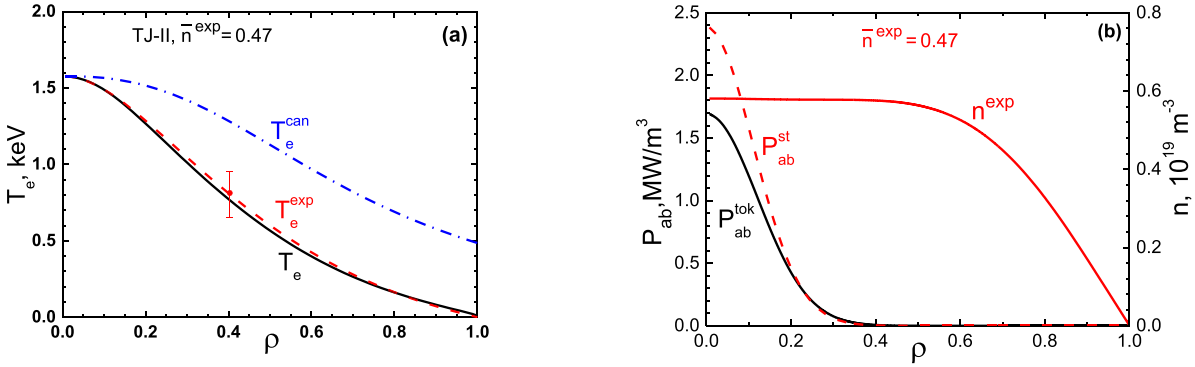

Figure 4. Modelling versus experiment for TJ-II shot #2047. (a) Electron temperature profiles, d2T_e = 2.8%; (b) density and the absorbed ECRH power density profiles P_{ab}^{st} ($\gamma = 0.11$) and P_{ab}^{tok} ($\gamma = 0.12$) for TJ-II shot #2047 and T-10V shot #2047t, $Q_{ab} = 0.18$ MW and $\eta^{st} = 0.38$.

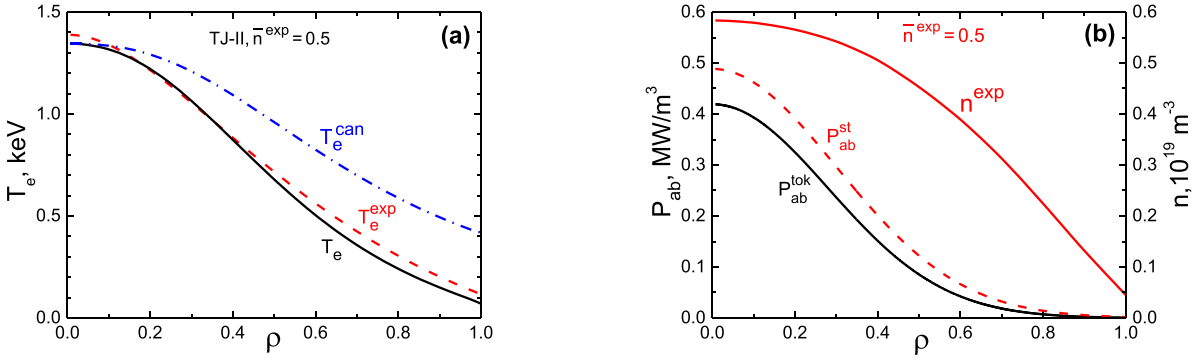

Figure 5. Modelling versus experiment for TJ-II shot #3050. (a) Electron temperature profiles, the deviation is d2T_e = 11%; (b) density and the absorbed ECRH power density profiles, $\gamma = 0.3$ and 0.28, $Q_{ab} = 0.22$ MW and $\eta^{st} = 0.47$.

T_e is the calculated profile of the electron temperature for T-10V;
T_e^{can} is the canonical profile of the electron temperature for T-10V;
P_{ab}^{st} is the profile of absorbed ECRH power density in TJ-II;
P_{ab}^{tok} is the profile of absorbed ECRH power density, determined by solving the inverse problem for T-10V;
η^{st} is the heating efficiency for TJ-II.

Figures 3–8 shows experimental T_e and n profiles for TJ-II shots from table 1 together with calculations for the equivalent tokamak T-10V shots, presented in table 2.

8. Empirical formulas for the ECR heating efficiency

Let us now construct the dependence of ECRH efficiency on the average plasma density for the T-10 tokamak and the TJ-II

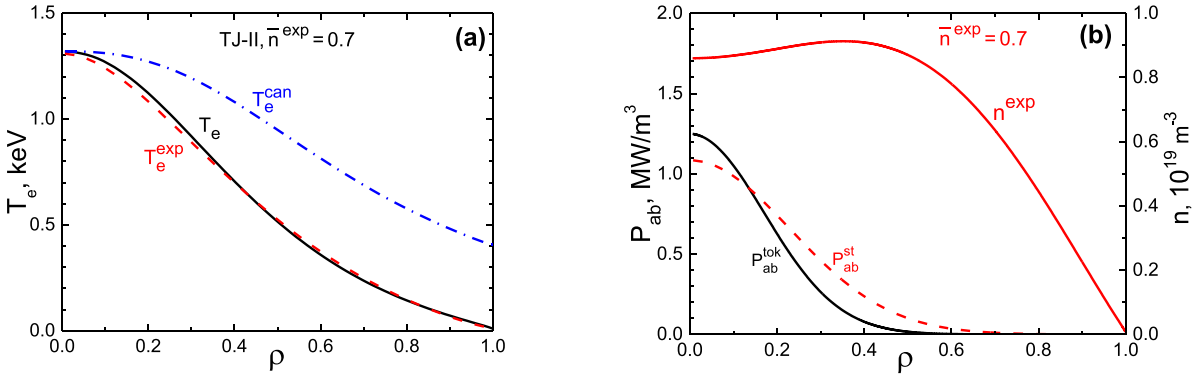

Figure 6. Modelling versus experiment for TJ-II shot #4070. (a) Electron temperature profiles. The deviation is d2T_e = 3.1%; (b) density and the absorbed ECRH power density profiles, $\gamma = 0.2$ and 0.17, $Q_{ab} = 0.25$ MW and $\eta^{st} = 0.53$.

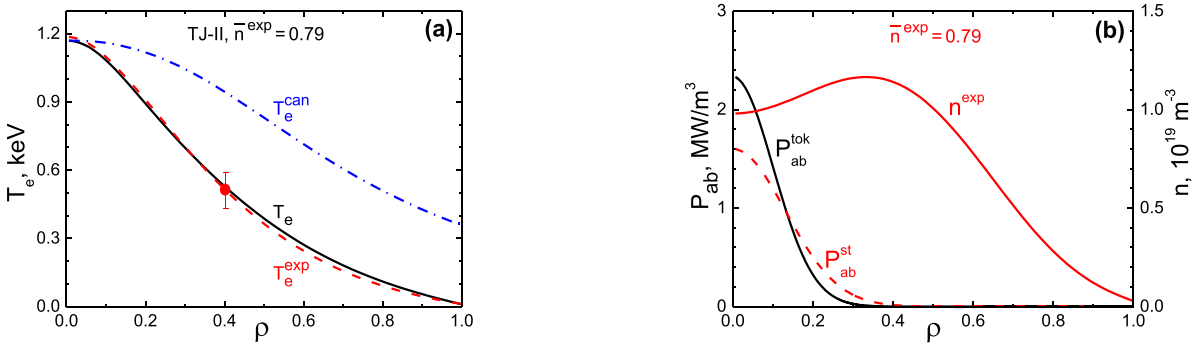

Figure 7. Modelling versus experiment for TJ-II shot #5079. (a) Electron temperature profiles. The deviation is d2T_e = 1.1%; (b) Density and the absorbed ECRH power density profiles, $\gamma = 0.15$ and 0.1, $Q_{ab} = 0.21$ MW and $\eta^{st} = 0.83$.

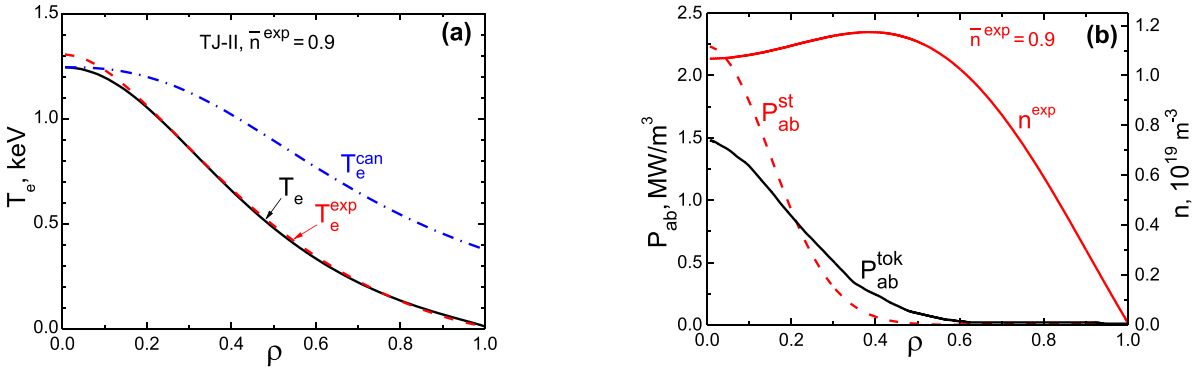

Figure 8. Modelling versus experiment for TJ-II shot #6090. (a) Electron temperature profiles. The deviation is d2T_e = 2.3%; (b) density and the absorbed ECRH power density profiles, $\gamma = 0.15$ and 0.17, $Q_{ab} = 0.30$ MW and $\eta^{st} = 0.63$.

stellarator. Figure 9(a) shows the T-10 shots on the plane ($\bar{n}$, η) with black squares, and the TJ-II shots with red circles. The empirical formula for the heating efficiency η was constructed based on T-10 results (with $B = 2.4$ T) and dimensional relations [4]:

$$\begin{aligned} &\eta = 2\,(\omega_p/\omega_B)^2 \quad \text{at } (\omega_p/\omega_B)^2 < 0.5 \quad \text{(partial absorption)} \\ &\eta = 1 \quad\quad\quad\quad \text{at } 0.5 < (\omega_p/\omega_B)^2 < 2 \quad \text{(full absorption)} \\ &\eta = 0 \quad\quad\quad\quad \text{at } 2 < (\omega_p/\omega_B)^2 \quad\quad \text{(cut-off condition)} \end{aligned} \tag{8}$$

where

$$\omega_p = \sqrt{\frac{4\pi\bar{n}e^2}{m}} \quad \text{and} \quad \omega_B = \frac{eB}{mc}$$

are the plasma and electron cyclotron frequencies.

Note that for the partial absorption (the top line of system (8)), $\eta \sim \bar{n}/B^2$. In figure 9(a), the thin dotted polyline shows the prediction by (8) for the heating efficiency in the TJ-II shots at $B = 1$ T. However, the experimental points from TJ-II (red circles) are systematically displaced from the dotted

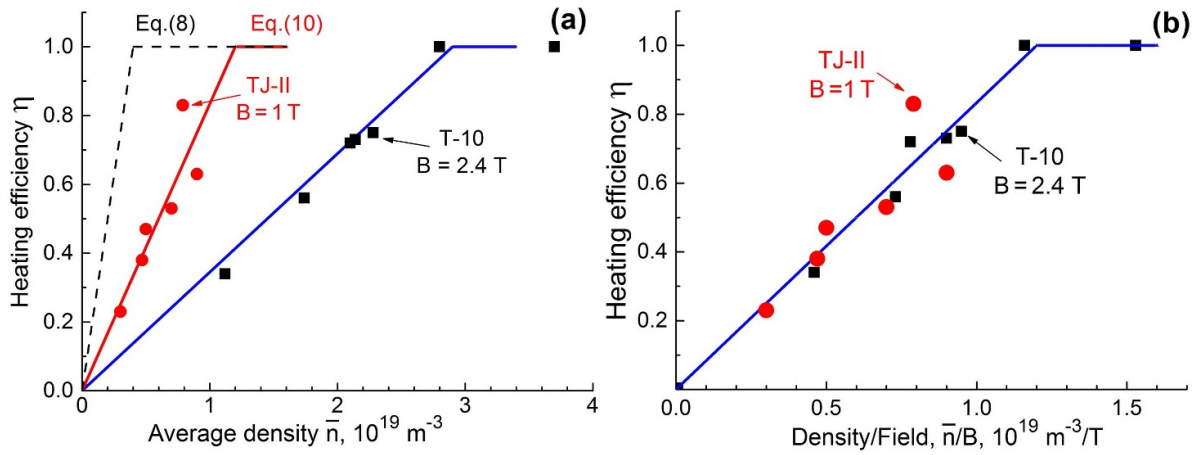

Figure 9. Absorption efficiency for the T-10 tokamak and TJ-II stellarator discharges versus line-averaged plasma density $\bar{n}$ (a), and on the ratio $\bar{n}/B$ (b). Red circles represent the experimental values of the heating efficiency for TJ-II and black squares for T-10. Thin dashed line and red solid line in (a) are predicted heating efficiency for TJ-II according to formulas (8) and (10a, 10b); blue solid polyline is predicted heating efficiency for T-10 according both to (8) and (10a, 10b).

line. This means that dependence $\eta \sim B^{-2}$ does not work and the η dependence on the magnetic field is weaker. It looks natural to try the linear inverse relationship:

$$\eta = \alpha \bar{n}/B, \tag{9}$$

where the parameter α is determined by the saturation density $\bar{n} = 3$ in figure 9(a) on the solid blue line for T-10 discharges, resulting in $\alpha = 0.83$.

Thus, more correct empirical formulas are given by:

$$\eta = \bar{n}/\bar{n}_{\rm cr} \quad \text{for } \bar{n} < \bar{n}_{\rm cr} \quad \text{(partial absorption)} \tag{10a}$$

$$\eta = 1 \quad \text{for } \bar{n} > \bar{n}_{\rm cr} \quad \text{(full absorption)} \tag{10b}$$

$$\eta = 0 \quad \text{for } n > n_{\rm cut}, \ \text{(cut-off condition)}, \tag{10c}$$

where $\bar{n}_{\rm cr} = B/0.83 = 1.2\ B$ (B in Tesla, n in 10^{19} m^{-3}), $n_{\rm cut}$ is the cut-off density, above which EC waves of X2 type do not propagate. Note that formulas (10a, 10b, 10c) cannot be written in dimensionless form.

Note that formulas (10a, 10b, 10c) are not in line with the classical formulas for the optical thickness. In our previous work [4] we estimated the plasma optical thickness τ in T-10 at $\bar{n} = 2 \times 10^{19}$ m^{-3} by the Prater's formula [23] (or formula (11) in [4]) as $\tau \sim 20$. Similar estimates for TJ-II: $\bar{n} \sim 1 \times 10^{19}$ m^{-3}, $T_{\rm e} \sim 1$ keV, R =1.5 m (the same as in T-10), $B = 1$ T, so λ (the EC-wavelength) is two times larger than in T-10 that gives $\tau \sim 10$. Therefore, for both machines classical formulas for optical thickness predict the single-pass absorption with efficiency $\eta = 1$ that contradicts to the observations, expressed by formulas (10a, 10b).

In figure 9(a), the red line predicts the heating efficiency of the TJ-II shots, according to formulas (10a). We can see that all the points are located near the red line. Thus, the empirical formulas (10a) are confirmed by experiments on two devices, TJ-II and T-10, with different magnetic fields, but with equal major radii.

In figure 9(b), the same points as in figure 9(a) are shown as the function of the ratio $\bar{n}/B$. We see that all experimental points from both machines are in line with formula (10a). The cut-off density for TJ-II with $B = 1$ T is $\bar{n}_{\rm cut} = 1.6 \times 10^{19}$ m^{-3}, while for T-10 with $B = 2.4$ T, it is much higher, $n_{\rm cut} = 12 \times 10^{19}$ m^{-3}.

9. Stored energy and confinement time in equivalent tokamak and stellarator discharges

We remind that the plasma densities and electron temperatures, as well as the absorbed powers in equivalent shots, must coincide. However, the plasma parameters that contain spatial variables (meters) in their dimensions might be different. These are the stored energy $W \propto nTV$, the energy confinement time $\tau_{\rm E} \propto nTV/Q_{\rm ab}$, the absorbed power density $Q_{\rm ab}/V$, and the volume V (m^3). This is because such parameters are calculated for an equivalent tokamak with its spatial dimensions. The spatial dimensions of the stellarator and tokamak having equivalent shots can be different. Therefore, in the above figures, the electron temperatures and absorbed power values in equivalent discharges are the same in the normalized coordinates, with discrepancies $\leqslant 10\%$, see figures 3–8. At the same time, power densities and effective thermal diffusivity coefficients are calculated for an equivalent tokamak, while they must be recalculated for an equivalent stellarator. Since in this particular case the major radii of equivalent discharges are the same, the multiplier (or divider) for recalculation is the ratio of the squares of the effective radii of the stellarator $a_{\rm eff}$ and the minor radius of the tokamak $a_{\rm tok}$:

$$\xi = (a_{\rm eff}/a_{\rm tok})^2. \tag{11}$$

Table 3. Global plasma parameters for equivalent tokamak T-10V shots.

No. shot	W_e, kJ	W_i, kJ	W_{tot}, kJ	Q_{ab}^{tok}, MW	$\bar{n}$, 10^{19} m^{-3}	τ_E ms
1030t	0.81	0.13	0.94	0.11	0.30	8.5
2047t	1.3	0.26	1.56	0.18	0.47	8.7
3050t	1.7	0.28	2.0	0.22	0.50	9.0
4070t	1.8	0.5	2.3	0.25	0.70	9.2
5079t	1.6	0.57	2.2	0.21	0.79	10
6090t	2.2	0.8	3.0	0.30	0.90	10

Table 4. Global plasma parameters for TJ-II shots.

No. shot	W_e, kJ	W_i, kJ	W_{tot}, kJ	Q_{ab}^{st}, MW	$\bar{n}$, 10^{19} m^{-3}	τ_E, ms
1030	0.43	0.07	0.50	0.11	0.30	4.5
2047	0.69	0.14	0.83	0.18	0.47	4.6
3050	0.90	0.15	1.05	0.22	0.50	4.75
4070	0.96	0.26	1.22	0.25	0.70	4.78
5079	0.74	0.3	1.04	0.21	0.79	5.3
6090	1.16	0.42	1.58	0.30	0.90	5.3

Then the absorbed power density P_{ab}^{st} is recalculated as follows

$$P_{ab}^{st} = P_{ab}^{tok}/\xi. \tag{12}$$

The stored plasma energy of the stellarator W_{st} and the equivalent tokamak W_{tok} are related by the expression

$$W_{st} = \xi W_{tok}. \tag{13}$$

Since $a_{eff} = 0.22$ m and $a_{tok} = 0.3$ m, then $\xi = 0.53$.

Table 3 shows the calculation results of the energy characteristics of equivalent tokamak discharges. The STMCP model with classical formula of energy exchange between electrons and ions was used to calculate the stored ion energy W_i.

Here, W_e and W_i are the stored energies in the electron and ion components, $W_{tot} = W_e + W_i$, Q_{ab} is defined by equation (5), calculated for the equivalent tokamak T-10V shots, and the energy confinement time τ_E is defined as

$$\tau_E = W_{tot}/Q_{ab}. \tag{14}$$

Using (11), (13) and (14), we determine the similar characteristics for stellarator shots (table 4).

Figures 5(a)–(c) show the dependencies of absorbed power, total plasma stored energy and the energy confinement time τ_E on the average plasma density for the TJ-II shots. It shows that the τ_E weakly depends on the density and has a value of about 5 ms, because both the stored energy and absorbed power increase slightly with increasing density, and their ratio is almost constant.

The dependence of τ_E on density in TJ-II was considered several times [20, 24, 25]. However, [20] and [24] considered

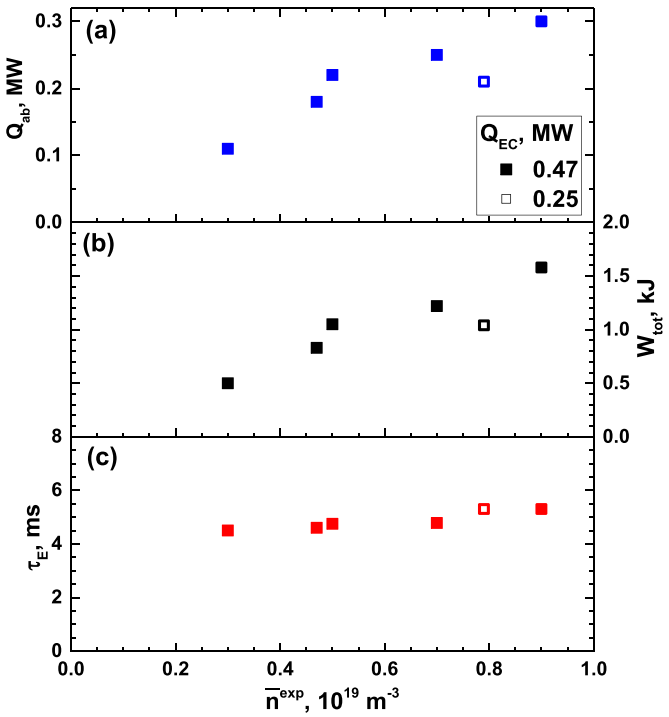

Figure 10. The absorbed power Q_{ab} (a); the total stored energy $W_{tot} = W_e + W_i$ (b); and the energy confinement time τ_E (c) as functions of the average plasma density in TJ-II. Open squares are for $Q_{EC}^{st} = 0.25$ MW, closed squares are for $Q_{EC}^{st} = 0.47$ MW.

fixed heating efficiency, despite it might be affected by density variation [22]. These estimates of τ_E generally include a fixed reduction of the nominal ECRH power and yield values roughly in the range 2–4 ms. The larger, approximately constant values of τ_E in figure 10, are a consequence of the dependence of the heating efficiency shown in figure 9(a). ECRH experiments in the TJ-II showed a heating efficiency around 0.5 for $\bar{n}_e \sim 0.6$–0.7×10^{19} m^{-3} [26], similar to the values indicated in figure 9(a). Therefore, it is suggested that electron energy confinement times in TJ-II require estimations of η in the appropriate range of densities studied.

10. Discussion

Now, we consider the range of applicability the expression (1). It was shown in [4] that it is valid for W7-X and T-15MD. To estimate the applicability of (1) it is enough to show that for other stellarators with different sizes and shapes, magnetic fields, densities, different character of power absorption and different $\iota(a)$, the expression (1) supports the temperature equality to the equivalent discharges. This equality in six discharges of the TJ-II stellarator with partial absorption is shown here. As a result, the expression (1) is supposed to be valid for the stellarators with wide range of parameters. In particular, it

should be checked, whether it is the only edge rotational transformation that matters, or may be a combination of magnetic shear and rotational transform must be considered (both W7-X and TJ-II are characterized by the low vacuum magnetic shear). This is left for future study.

Here we discuss L-mode plasmas heated at the second ECRH harmonic. The concept of equivalence of stellarator and tokamak shots for the case of fully absorbed ECRH power was formulated in [4]. The solution of the direct problem for the STMCP model shows that the electron and ion temperatures are pairwise the same for equivalent discharges.

Is it possible to extend the concept of equivalence to the partial absorption? This paper provides a positive but somewhat complex answer. The main difficulty is the formulation of the equivalence conditions. We require, in addition, that the electron temperature in the stellarator is experimentally measured. In this case, we have to solve the inverse problem by the STMCP model. However, the inverse problem is ill-posed, and in the usual sense, it has no solution. To overcome this issue, we improved the procedure proposed in [4] by restricting the allowable functions to a certain class, enabling us to solve the inverse problem.

In particular, we show how to regularize the inverse problem so that the constructed quasi-solution is physically meaningful. A simple two-parameter class of allowable functions was chosen for the profile of the power absorbed by the electrons. As a result, the RMS difference between the optimal electron temperature profile found for the tokamak and the measured electron temperature in the stellarator is only a few percent. Thus, even in the case of partial absorption of the ECRH power, in an equivalent pair of discharges, the respective electron temperatures and absorbed powers are practically the same.

The requirements for the equivalence of discharges does not include the requirement of equal volumes. As the plasma volume decreases from $V_{\max}$ to $V_{\min}$ (with fixed absorbed power), the power deposition to the electrons increases in proportion to the volume ratio $V_{\max}/V_{\min}$. At the same time, the energy confinement worsens in the same ratio [3], and this experimental fact coincides with the predictions of the STMCP model. As a result, both processes compensate mutually and the electron temperature remains unchanged (in normalized coordinates, of course). We have shown in [4] that this fact is physically meaningful, because at the same heating power in W7-X and T-15MD (5 MW) and very different plasma volumes, the temperature of both electrons and ions is the pairwise the same. This compensation is the reason, why the equivalence conditions do not include the plasma geometry and dimension.

Generally, the ECRH X2 power absorption depends on plasma density, electron temperature and magnetic field [23]. These parameters are not independent, they are coupled to each other and with others parameters, for example, with the input power Q_{EC}.

According to equation (10b), if $\bar{n} > n_{\mathrm{cr}}$, the full absorption is realized, independently on T_{e} or ECRH power Q_{EC}, $\eta = 1$. In the opposite case, $\bar{n} < n_{\mathrm{cr}}$, there are two different regimes, separated by T_{e} (or input power Q_{EC}). If T_{e} is large enough, or Q_{EC} is higher than some critical power Q_{cr}, $Q_{\mathrm{EC}} > Q_{\mathrm{cr}}$, then the full absorption is realized, $\eta = 1$. Otherwise, $Q_{\mathrm{EC}} < Q_{\mathrm{cr}}$, the partial absorption takes place, as we have observed for TJ-II, see equation (10a) and figure 9. Here, there are no T_{e} effect observed and the only plasma density affects the absorption efficiency. Such a regime for T-10 is considered in [4] as the regime with threshold temperature. It is also realized for TJ-II, see figure 2. For this regime, the increase of the input power Q_{EC} increases the temperature T_{e}, but keeps the absorption efficiency. Figure 9 shows that in this regime the heating efficiency differs from equation (8) and follows equations (10a, 10b).

Finally, the concept of the equivalent tokamak-stellarator discharges, suggested in [4], is valid for both full and partial ECRH power absorption. As an outcome of the equivalence conditions, heating efficiencies were analyzed.

Therefore, based on the equivalence criterion (e), we may state that in the L-mode the energy transport characteristics in a stellarator are the same as in a tokamak with different magnetic helicity (by a factor of $\sim$6 smaller) near the plasma boundary.

11. Conclusion

Using the principle of equivalence of stellarator and tokamak discharges and the STMCP, the energy balance in series of TJ-II stellarator discharges is analyzed. The values of the absorbed power and its radial distribution are found. In the whole considered density range $(0.3 < \bar{n} < 0.9) \times 10^{19}$ m^{-3}, the input EC-power absorption efficiency is $0.2 < \eta < 0.82$. A new empirical formula for the ECRH efficiency is suggested. This formula confirms the equality of the energy transport in the equivalent shots of stellarator and tokamak. Thus, the energy transport similarity in the equivalent discharges of stellarator and tokamak is confirmed not only for full, but for partial absorption of ECRH power as well.

Data availability statement

The data generated and/or analysed during the current study are not publicly available for legal/ethical reasons but are available from the corresponding author on reasonable request.

Acknowledgments

Authors are grateful to Dr I Pastor for providing the Thomson Scattering data and to the TJ-II team for long-term collaboration. Y N Dnestrovskij and D Y Sychugov were supported by RFBR Grant 20-07-00391, A V Melnikov is partly supported by the Competitiveness Program of NRNU MEPhI. T-10 experiments were supported by the Federal project 'Development of controlled nuclear fusion technologies and innovation

plasma technologies'. Order NRC KI No. 2996 at 31 December 2020.

Appendix A. Brief description of the Standard Transport Model of Canonical Profiles

The discussed STMCP model is implemented into the ASTRA code [27]. At the initial stage of the code running, the Grad-Shafranov equation is solved, and the equilibrium and natural coordinates are found within a fixed plasma boundary. The radial coordinate ρ is defined from the toroidal magnetic flux. It is assumed that the canonical temperature profiles for electrons and ions can be different [28]:

$$\Gamma_\alpha = -k_\alpha^{\mathrm{PC}} T_\alpha \left(\frac{T'_\alpha}{T_\alpha} - \frac{T'_{c\alpha}}{T_{c\alpha}} \right) (\alpha = e, i), \tag{A1}$$

where $T_{c\alpha}$ is the canonical temperature profile of the α–sort particles. Here $T'_\alpha = \mathrm{d}T_\alpha/\mathrm{d}\rho$. Also we assume that the stiffness coefficients for the electron and ion temperatures k_α^{PC} have the form

$$\begin{aligned} k_\alpha^{\mathrm{PC}} &= n\chi_\alpha^{\mathrm{PC}} \\ &= C_\alpha \frac{1}{M} \left(\frac{a}{R}\right)^{0.75} q_{\mathrm{cyl}}\, q\left(\rho = \frac{\rho_{\max}}{2}\right) \left(T_\alpha\left(\rho = \frac{\rho_{\max}}{4}\right)\right)^{h_\alpha} \\ &\quad \times \left(\frac{3}{R}\right)^{1/4} \left(\frac{\bar{n}}{B}\right) \\ &= \mathrm{const}(\rho). \end{aligned} \tag{A2}$$

Here k_α^{PC} in $\mathrm{m}^{-1}\,\mathrm{s}^{-1}$, $\chi_\alpha^{\mathrm{PC}}$ in $\mathrm{m}^2\,\mathrm{s}^{-1}$, C_α and h_α are numerical coefficients, M is the relative mass of the ion, T_α is the temperature in keV, a and R are minor and major plasma radii in meters, B is the toroidal magnetic field in T, $q_{\mathrm{cyl}} = 5a^2B/(IR)$, ρ is the radial coordinate of the flux surface, $\rho_{\max}$ is the value of ρ on the plasma boundary, I is the plasma current in MA.

According to [28–30], the canonical profile for the function $\mu(\rho) = 1/q(\rho)$ is defined by the following Euler equation

$$\begin{aligned} &\rho^2 G \frac{\partial \mu_\alpha^2}{\partial \rho} + \lambda_\alpha \frac{\partial}{\partial \rho}\left[\frac{1}{V'}\frac{\partial}{\partial \rho}(V' G \rho \mu_\alpha)\right] + \frac{D_\alpha \rho}{V'}\frac{\partial \mu_\alpha}{\partial \rho} \\ &\quad = 0\ (\alpha = e, i). \end{aligned} \tag{A3}$$

These are two separated second-order nonlinear equations with two unknown parameters λ_α and D_α for each equation (Lagrange parameters), so four following boundary conditions are required to find a unique solution for each equation [13, 14]:

$$\begin{aligned} &\mu_\alpha(0) = \mu_{0\alpha}, \quad \mu'_\alpha(0) = 0, \quad \mu_\alpha(\rho_{\max}) = \mu_{\mathrm{a}}, \\ &\frac{\mu_{0\alpha}}{2}\frac{i_{\alpha \mathrm{a}}}{G_{\mathrm{a}}\mu_{\mathrm{a}}^2} = U_\alpha, \end{aligned} \tag{A4}$$

where $\mu_{\mathrm{a}} = 1/q(\rho_{\max})$. We will denote the solution of problem (A3) and (A4) by the index 'c' below, i_α in (A4) is a dimensionless canonical current profile defined by:

$$i_\alpha = \mathrm{rot}_\varphi(\rho\mu_\alpha) = \frac{1}{V'}\frac{\partial}{\partial \rho}(V' G \rho \mu_\alpha), \tag{A5}$$

which is a formal parameter of the STMCP, and it may be different for electrons and ions. In (A3)–(A5), G is a dimensionless metric coefficient defined by

$$G = G(\rho) = R^2 \left\langle \frac{(\nabla \rho)^2}{r^2} \right\rangle, \tag{A6}$$

where the parentheses <…> mean averaging over the magnetic surface, r is the distance from the current point at the magnetic surface to the major axis of the torus, $V' = \partial V/\partial \rho$, V is the plasma volume inside the magnetic surface, U_α is a certain constant equal to unity for a circular plasma cylinder, and defined in the general case as [13, 14]:

$$\frac{\partial Z_\alpha(\rho)}{\partial \rho}(\rho = \rho_{\max}) = 0, \tag{A7}$$

where

$$Z_\alpha(\rho) = \frac{\mu_{0\alpha}}{2}\frac{i_{c\alpha}(\rho)}{G(\rho)(\mu_{c\alpha}(\rho))^2}. \tag{A8}$$

Condition (A7) should be added to the boundary conditions (A4).

Canonical profiles for temperature are determined by Ohm's law, accounting Spitzer conductivity, which has the form

$$T_{c\alpha}(\rho) = (i_{c\alpha}(\rho))^{2/3}. \tag{A9}$$

For circular plasma with a large aspect ratio ($R/a \gg 1$), the relations between variables are simplified

$$i_{c\alpha} = (\mu_{c\alpha})^2, T_{c\alpha} = (\mu_{c\alpha})^{4/3}. \tag{A10}$$

Equation (A3) with boundary conditions (A4) and (A7) should be solved separately for electrons and ions, choosing the corresponding values of $\mu_{0\alpha}$ and determining the parameters λ_α and C_α in the course of solving equation (A3) by the iterative method. The heat transport equations have the form of energy conservation

$$\frac{3}{2}\frac{\partial}{\partial t}(nT_\alpha) + \frac{1}{V'}\frac{\partial}{\partial \rho}(V' G_1 \Gamma_\alpha) = P_\alpha, (\alpha = e,\ i) \tag{A11}$$

where P_α are the heat sources, $G_1 = \left\langle (\nabla \rho)^2 \right\rangle$.

We estimate the model accuracy with the root-mean-square (RMS) difference $d2T_\alpha$ between the calculated electron or ion temperature profile T_α and the experimental temperature profile T_α^{exp}.

$$d2T_\alpha = \left(\int_0^{0.7} \mathrm{d}\rho\, \frac{(T_\alpha - T_\alpha^{\mathrm{exp}})^2}{(T_\alpha^{\mathrm{exp}})^2} \Big/ \int_0^{0.7} \mathrm{d}\rho \right)^{1/2}. \tag{A12}$$

Table A1. The STMCP coefficients.

C_e	μ_{0e}	C_i	μ_{0i}
3.5	0.6	3.8	0.5

The heat fluxes (A1), (A2) and canonical profiles contain the following six coefficients

$$\mu_{0e}, \mu_{0i}, C_e, C_i, h_e, h_i. \tag{A13}$$

Not all of them are independent in their effect on the energy transport. C_α and h_α determine the coefficients k_α^{PC}, so one of these two can be set constant; μ_{0e} and μ_{0i} determine the shape of the canonical electron and ion temperature profiles, so we leave them free. Thus, we assume

$$h_e = 0.5,\ h_i = 0.5, \tag{A14}$$

and we leave two coefficients for electrons to vary

$$\mu_{0e} \text{ and } C_e \tag{A15}$$

and two coefficients for ions

$$\mu_{0i} \text{ and } C_i. \tag{A16}$$

To determine these coefficients, we model the selected T-10 database, having 10 shots with $3 < q_a < 5.5$ [4]. As a result, we complete the STMCP with full set of coefficient in the table A1.

Appendix B. Table of TJ-II discharges

Table A2. TJ-II discharges used to get the averaged electron temperatures.

Symbolic number	Average density $\bar{n}$, 10^{19} m^{-3}	TJ-II discharge numbers
1030	0.30	48 094, 48 107
2047	0.47	48 406, 48 410, 48 415, 48 417, 48 431, 48 432
3050	0.50	48 127, 48 126, 48 125, 48 615, 48 546, 48 539, 48 506, 48 555, 48 121, 48 507, 48 554, 50 320
4070	0.70	48 503, 48 541, 48 154, 48 537, 48 549, 48 210, 48 145
5079	0.79	48 418, 48 412, 48 426, 48 435, 48 441
6090	0.90	48 217, 48 522, 48 091, 48 212, 48 223, 48 525, 48 511, 48 519, 48 219, 48 521

ORCID iDs

A V Melnikov https://orcid.org/0000-0001-6878-7493
D Lopez-Bruna https://orcid.org/0000-0002-7638-8772
A Yu Dnestrovskij https://orcid.org/0000-0002-4827-9421
L G Eliseev https://orcid.org/0000-0002-2787-2103
P O Khabanov https://orcid.org/0000-0002-6004-2005
S E Lysenko https://orcid.org/0000-0003-1529-2088

References

[1] Stroth U 1998 A comparative study of transport in stellarators and tokamaks *Plasma Phys. Control. Fusion* **40** 9

[2] Imbeaux F, Ryter F and Garbet X 2001 Modelling of ECH modulation experiments in ASDEX Upgrade with an empirical critical temperature gradient length transport model *Plasma Phys. Control. Fusion* **43** 1503

[3] Stroth U *et al* 2021 Stellarator-tokamak energy confinement comparison based on ASDEX Upgrade and Wendelstein 7-X hydrogen plasmas *Nucl. Fusion* **61** 016003

[4] Dnestrovskij Y N *et al* 2021 Transport model of plasma heating at the second harmonic of the electron-cyclotron frequency *Plasma Phys. Control. Fusion* **63** 055012

[5] Klinger T *et al* 2019 Overview of first Wendelstein 7-X high performance operation *Nucl. Fusion* **59** 112004

[6] Dnestrovskij Y N *et al* 2020 Comparison of plasma heating at first and second electron cyclotron harmonics in the T-10 tokamak *Plasma Phys. Rep.* **46** 477–89

[7] Dinklage A *et al* 2013 Inter-machine validation study of neoclassical transport modelling in medium- to high-density stellarator-heliotron plasmas *Nucl. Fusion* **53** 063022

[8] Bozhenkov S A *et al* 2019 Characterization of the collisional transport of a high-Z impurity in a Wendelstein 7-X electron cyclotron resonance heated plasma *Proc. 61st Annual Meeting APS Division of Plasma Physics* vol 64 (*Fort Lauderdale, Florida, USA*, *21–25 October 2019*) p YP10.00058 (available at: http://meetings.aps.org/Meeting/DPP19/Session/YP10.58)

[9] Hirsch M *et al* 2008 Major results from the stellarator Wendelstein 7-AS *Plasma Phys. Control. Fusion* **50** 053001

[10] Melnikov A V *et al* 2007 Pressure profile shape constancy in L-mode stellarator plasmas *34th EPS Conf. on Plasma Physics* vol 32F (*Warsaw*, *2–6 July 2007*) (ECA) p P2_060 (available at: http://ocs.ciemat.es/EPS2007/pdf/P2_060.pdf)

[11] Dnestrovskij Y N, Melnikov A V and Pustovitov V D 2009 Approach to canonical pressure profiles in stellarators *Plasma Phys. Control. Fusion* **51** 015010

[12] Eliseev L G *et al* 2021 Experimental observation of the geodesic acoustic frequency limit for the NBI-driven Alfvén eigenmodes in TJ-II *Phys. Plasmas* **28** 072510

[13] Dnestrovskij Y N 2015 *Self–Organization of Hot Plasmas* (Switzerland: Springer) (https://doi.org/10.1007/978-3-319-06802-2)

[14] Dnestrovskij Y N, Connor J W, Cherkasov S V, Danilov A V, Dnestrovskij A Y, Lysenko S E, Roach C M and Walsh M 2007 Analysis of pressure profiles and transport simulations of MAST discharges *Plasma Phys. Control. Fusion* **49** 1477–96

[15] Andreev V F *et al* 2016 Experimental study of density pump-out effect with on-axis electron cyclotron resonance heating at the T-10 tokamak *Plasma Phys. Control. Fusion* **58** 055008

[16] Andreev V F and Kas'yanova N V 2005 Accuracy of reconstruction of the transport coefficients and ECRH power profile in tokamaks from solutions to inverse problems *Plasma Phys. Rep.* **31** 720

[17] Golant V E and Feodorov V I 1986 *High Frequency Methods of Plasma Heating in Toroidal Thermonuclear Devices* (Moscow: Energoatomizdat)

[18] Martinez-Fernandez J, Cappa Á, Tereshchenko M, Tolkachev A, Ros A and Catalán G 2020 High power characterisation of the ECRH transmission lines and power deposition calculations in the TJ-II stellarator *Fusion Eng. Design* **161** 112065

[19] Alejaldre C *et al* 1990 TJ-II project: a flexible heliac stellarator *Fusion Sci. Technol.* **17** 131–9

[20] Gutierrez-Tapia C *et al* 2015 Analysis of TJ-II experimental data with neoclassical formulations of the radial electric field *Plasma Phys. Control. Fusion* **57** 115004

[21] Melnikov A V, Dyabilin K S, Eliseev L G, Lysenko S E and Dnestrovskij Y N 2011 Measurement and modelling of electric potential in the TJ-II stellarator *Probl. At. Sci. Technol. Ser. Thermonuclear Fusion* **3** 54–73

[22] Ascasibar E, Estrada T, Castejón F, López-Fraguas A, Pastor I, Sánchez J, Stroth U, Qin J and TJ-II Team 2005 Magnetic configuration and plasma parameter dependence of the energy confinement time in ECR heated plasmas from the TJ-II stellarator *Nucl. Fusion* **45** 276–84

[23] Prater R 2004 Heating and current drive by electron cyclotron waves *Phys. Plasmas* **11** 2349

[24] Vargas V I *et al* 2006 Density dependence of particle transport in ECH plasmas of the TJ-II stellarator *Tech. Rep. 1079* (CIEMAT) (available at: https://inis.iaea.org/collection/NCLCollectionStore/_Public/40/044/40044726.pdf?r=1)

[25] Lopez-Bruna D *et al* 2021 Plasma electric potential in the TJ-II stellarator: neoclassical formulation versus measurements *Probl. At. Sci. Technol. Ser. Thermonuclear Fusion* **44** 91–105 (available at: http://vant.iterru.ru/engvant_2021_1.htm)

[26] Eguilior S, Castejón F, de la Luna E, Cappa A, Likin K, Fernández A and TJ-II Team 2003 Heat wave experiments on TJ-II flexible heliac *Plasma Phys. Control. Fusion* **45** 105–20

[27] Pereverzev G V and Yushmanov P N 2002 ASTRA an Automated System for TRansport Analysis *IPP Report* 5/42 (Max-Planck-Institut für Plasmaphysik)

[28] Dnestrovskij Y N, Dnestrovskij A Y and Lysenko S E 2005 Self-organization of plasma in a tokamak *Plasma Phys. Rep.* **31** 529–53

[29] Kadomtsev B B 1986 Self-organization in a tokamak plasma *Radiophys. Quantum Electron.* **29** 781–7

[30] Dnestrovskij Y N, Dnestrovskij A Y, Lysenko S E and Cherkasov S V 2002 Canonical profiles in tokamak plasmas with an arbitrary cross section *Plasma Phys. Rep.* **28** 887–99